

pubs.acs.org/macroletters Letter

Diblock Rings as Topological Adhesives at Immiscible Polymer Interfaces

Andrew Wijesekera, Daniel L. Vigil, Gary S. Grest, Siteng Zhang, and Ting Ge*



Cite This: ACS Macro Lett. 2024, 13, 1311–1317



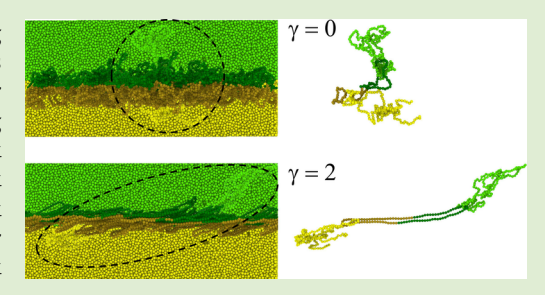
ACCESS I

III Metrics & More

Article Recommendations

Supporting Information

ABSTRACT: Disparate polymers often do not mix well, and the resulting immiscible interfaces are mechanically weaker than the bulk, which is undesirable for many technological applications. Large-scale molecular simulations are performed to demonstrate the effectiveness of diblock ring polymers as a new type of adhesive for immiscible polymer interfaces. The peak stress σ_p and the failure strain γ_p upon shear deformation approach the bulk values with increasing diblock ring length and coverage. Breaking the diblock rings into pairs of diblock linear chains creates a reference system for comparison. The diblock rings increase both σ_p and γ_p compared to the diblock linear chains at the same coverage. Further topological analysis based on the



Gauss Linking Number reveals that the threading of diblock rings by linear chains from the two opposite sides is the key mechanism for stronger adhesion, which is analogous to the hook-and-loop process in Velcro tape.

espite the ubiquity of polymer interfaces in heterogeneous polymeric materials, the immiscibility of most polymers results in limited interfacial mixing and mechanically weak interfaces. 1-3 Reinforcing immiscible polymer interfaces is necessary to promote mechanical integrity and benefit many applications, such as layer-by-layer 3D printing of polymers, recycling and upcycling of polymer blends, and fabricating polymer-based biomedical devices. Many strategies have been devised to promote polymer adhesion.4 Two major microscopic mechanisms underlying the strategies are creating chemical bonds at the interface between the two immiscible polymers and forming physical entanglements across the interface. One example is the reinforcement of an immiscible interface by block copolymers, 5-10 where the entanglements between the blocks and the homopolymers of the same type bridge the two sides of the interface.

Advances in chemical synthesis offer a promising avenue for constructing interfacial molecular bridges and enhancing polymer adhesion by manipulating polymer chain topology. 11,12 In this Letter, we propose and study a new microscopic mechanism for polymer adhesion based on the unique topology of ring polymers. We use molecular dynamics simulations to demonstrate that diblock ring polymers at the interface between two immiscible linear polymers act as topological adhesives that resemble the hook-and-loop process in Velcro tapes. When compared with diblock linear polymers, which rely on polymer entanglements to bridge immiscible polymers, diblock ring polymers may be threaded by linear chains from two sides of the interface, and the resulting ringlinear threading is more effective in promoting adhesion. The use of ring-linear threading for adhesive strength of polymer interface is a new addition to the cutting-edge research

portfolio exploring the unique topology of ring-linear threading, which covers the unconventional dynamics and rheological properties of ring and linear polymer blends^{13–15} and loopy single-chain nanoparticles¹⁶ in linear polymers.

Polymers are modeled using the canonical bead-spring model. All beads of size σ_{LJ} and mass m interact via the truncated and shifted 12-6 Lennard-Jones (LJ) potential with cutoff distance $r_c = 2.5\sigma_{LJ}$ and unit interaction strength ϵ . The characteristic time is $\tau = \sqrt{m\sigma_{LJ}^2/\epsilon}$. Adjacent beads on the polymer chain are linked by the finite extensible nonlinear elastic (FENE) bonding potential. A three-body bending potential $U(\theta) = k_{\theta}(1 + \cos \theta)$ is employed for two neighboring bonds along the polymer chain, where θ is the angle between the bonds. $k_{\theta} = 1.5\epsilon$ is used, which results in $N_{\epsilon} = 28$ for the entanglement length of linear polymer melts. All $k_{\theta} = 1.8$ for the entanglement length of linear polymer melts.

Two films consisting of polymers of types A and B, respectively, were constructed and brought into contact to generate an immiscible polymer interface. Each film contains M=2500 well-entangled polymer chains with $N=200\approx 7N_e$ beads per chain. Previous studies^{2,19} have shown that the mechanical strength of bulk polymers typically saturates around $N/N_e=10$. Both films were subject to periodic boundary conditions in the x- and y-directions with

Received: July 3, 2024
Revised: September 3, 2024

Accepted: September 11, 2024 Published: September 18, 2024





dimensions L_x and L_y . The two films were stacked along the nonperiodic z-direction and confined between two walls separated by L_z = 120.5 $\sigma_{\rm LJ}$. The LJ interaction strength $\epsilon_{\rm AA}$ = ϵ_{BB} = ϵ for the monomers of the same type, but is reduced to $\epsilon_{AB} = 0.9\epsilon$ for the monomers of different types. The monomers interact with the confining walls via the 9-3 LJ potential with cutoff distance $r_c = 0.858\sigma_{LJ}$. The system was equilibrated at temperature $T = 1.0\epsilon/k_B$ and pressure $P_x = P_y = 0$. The temperature was maintained using a Nosé-Hoover thermostat with a characteristic damping time 10τ , while the pressure was controlled by a Nosé-Hoover barostat with a characteristic damping time 100τ . To accelerate the equilibration, the "double bridging" algorithm²⁰ was used to bypass the limitation of slow entangled chain dynamics. All simulations were performed using the LAMMPS package²¹ with a time step of 0.01τ . The overall density of the monomers in the equilibrated sample is $0.86\sigma_{LJ}^{-3}$, with $L_x = 98.8\sigma_{LJ}$ and $L_y =$ $97.5\sigma_{LJ}$. The immiscible polymer interface at equilibrium has a sharp interface, as shown by the monomer density profile in Figure S1a of Supporting Information (SI). This justifies the selected value of ϵ_{AB} for immiscibility. The monomer density profiles for all systems in Figure S1 were averaged over 100 frames with an interval of $10^3\tau$ between two frames, corresponding to thermodynamic stability over $10^5\tau$. As a reference system, a bulk homopolymer consisting of M = 5000chains and N = 200 beads per chain was prepared with periodic boundary conditions in all three directions. For the equilibrated bulk sample, $L_x = 98.2\sigma_{LJ}$, $L_y = 98.1\sigma_{LJ}$, and $L_z =$ $120.5\sigma_{LI}$.

An immiscible polymer interface reinforced by diblock ring polymers was simulated by adding a layer of diblock rings between two immiscible polymer films. Each diblock ring of N_{db} monomers is symmetric with equal number of A and B monomers. The value of N_{db} and the number of diblock rings M_{db} were varied to generate 4 different systems, the parameters of which are listed in Table 1. To accommodate the diblock

Table 1. Parameters for Simulation Samples

system	diblock topology	N_{db}	M_{db}	L_x/σ_{LJ}	L_y/σ_{LJ}	L_z/σ_{LJ}
R100-48	ring	100	48	80.1	80.0	180.5
R100-480	ring	100	480	81.8	81.7	180.5
R200-48	ring	200	48	69.6	69.2	240.5
R200-240	ring	200	240	70.9	70.5	240.5
L50-96	linear	50	96	79.8	80.3	180.5
L50-960	linear	50	960	82.3	81.2	180.5
L100-96	linear	100	96	69.6	69.1	240.5
L100-480	linear	100	480	70.7	70.6	240.5

rings, L_z was increased to $180.5\sigma_{LJ}$ for $N_{db}=100$ and $240.5\sigma_{LJ}$ for $N_{db}=200$. These systems were equilibrated using protocols similar to the equilibration of the immiscible interface, with the double bridging algorithm applied only to the linear chains of the same type. The density profiles of monomers of different systems at equilibrium are shown in Figure S1b–e. Corresponding systems with diblock linear chains were made by cutting each diblock ring to two symmetric diblock linear chains, which preserves the areal density of AB junction points. The parameters for the equilibrated systems with diblock linear chains are listed in Table 1. As shown in the insets of Figure S1b–e, the monomer density profiles for the diblock linear chains are almost unchanged with respect to those for the diblock rings. Moreover, the sizes of the diblock linear chains

and the corresponding diblock rings are almost the same, as characterized by the three components of the radius of gyration $R_{\rm g,x}$, $R_{\rm g,y}$, and $R_{\rm g,z}$ in Table S1 of the SI. The two types of blocks in the diblock copolymers are well separated from each other in all systems. The coverage of diblock copolymers at the interface is not too high to lead to pure lamellar domains as in symmetric diblock copolymer melts. In Table S1, the average spacing between neighboring diblock copolymers $d=(L_xL_y/M_{db})^{1/2}$ is compared with $R_{\rm g,x}$ and $R_{\rm g,y}$. The values of the overlap parameter $\Omega=\pi R_{\rm g,x}R_{\rm g,y}/d^2$, which corresponds to the number of diblock copolymers sharing the same pervaded area, are also listed in Table S1.

After equilibration, each system was quenched from T = $1.0\epsilon/k_{\rm B}$ to $T=0.1\epsilon/k_{\rm B}$ over $9\times10^4\tau$. During quenching, the pressure components for the periodic directions were kept at 0. For a homopolymer melt, the glass transition temperature $T_{\rm g} \approx$ $0.48\epsilon/k_{\rm B}$. Therefore, $T=0.1\epsilon/k_{\rm B}$ is well below $T_{\rm g}$. The mechanical strength at $T = 0.1\epsilon/k_{\rm B}$ was assessed by performing a simple shear test, which mimics the lap-joint shear test.^{2,23} To enable bond breaking, the FENE bonds were replaced with quartic bonds of the same equilibrium bond length, as in previous coarse-grained simulations of polymer failure mechanics.^{23–25} The maximum force before the breaking of a quartic bond is 100 times larger than the maximum attractive force for the 12-6 LJ interaction. For the simple shear test, an upper layer and a lower layer, both of thickness $5\sigma_{Ll}$, were frozen as rigid bodies. In the systems with immiscible interfaces, the two layers were at the free surfaces of the two thin films. In the bulk system, the two layers lie across the periodic boundary in the z-direction. During the shearing of all systems, the two layers were displaced in opposite directions along the x-axis at a constant velocity $0.005\sigma_{LI}/\tau$, which corresponds to shear rates on the order of $10^{-4}\tau^{-1}$

The mechanical response of each sample is quantified by the shear stress-strain curve. The shear stress σ is calculated as the average force applied to the upper and lower frozen layers divided by the surface area L_xL_y . The shear strain γ is the relative displacement of the two layers along the x-direction divided by the spacing $(L_z - 10\sigma_{LI})$ between the layers. Figure 1 compares the stress-strain curves from shearing the immiscible polymer system and the bulk homopolymer. Also shown in Figure 1 is the fraction of broken bonds $f_{
m broken}$ as a function of γ in the two samples. The initial elastic response and yielding of the two samples overlap, while remarkably different postyield behaviors are observed at large γ . Both the peak stress σ_p and the corresponding failure strain γ_p for the immiscible polymer interface are significantly reduced compared to that of the bulk sample. The immiscible interface fails through catastrophic chain pullout, as illustrated in Figure 1b. Chains are easily pulled out without breaking any bonds, because the limited mutual interpenetration prevents the formation of polymer entanglements that can arrest the pullout. By contrast, the bulk sample fails through chain scission, as illustrated in Figure 1c. $f_{\rm broken}$ rises prior to the stress peak and saturates as σ drops toward the value for the friction at the fracture plane. The transition from the failure by chain pullout to the one by chain scission is enabled by the entanglement network in the bulk sample. 19,23,26 The entanglements between polymer chains are analyzed using the Z1+ package,²⁷ which identifies the kinks along the primitive paths of entangled chains. The inset in Figure 1a shows the number density of kinks ρ_K is much lower at the

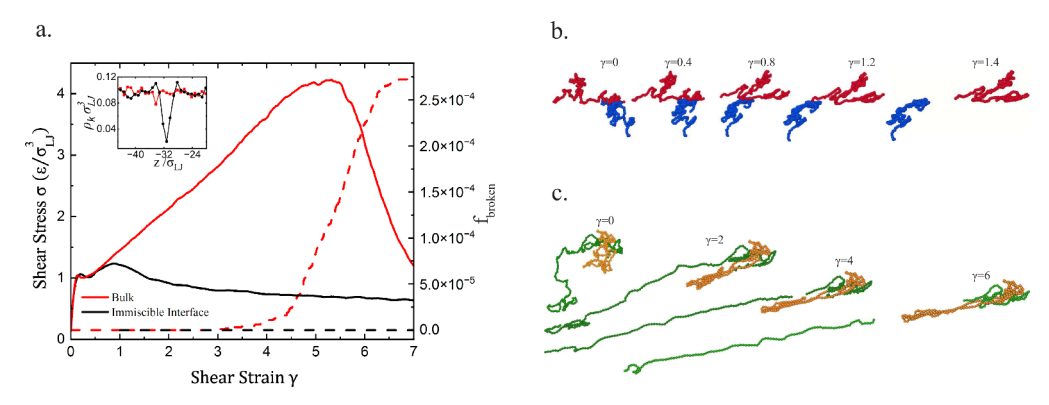


Figure 1. (a) Shear stress σ (solid) and the fraction of broken bonds f_{broken} (dashed) as functions of shear strain γ for the immiscible interface (black) and the bulk homopolymer (red). The inset shows the number density of kinks ρ_K as a function of z for the two systems. Visualization of the evolution of two polymer chains (b) at the immiscible interface and (c) in the bulk. The red and blue chains in (b) are of types A and B, respectively. The green and orange chains in (c) are entangled and of the same type.

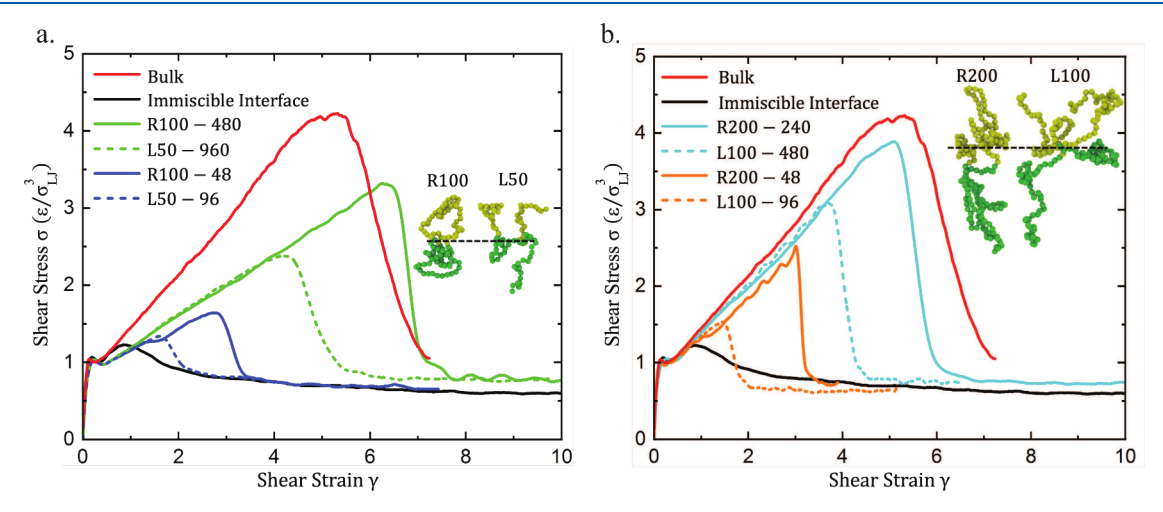


Figure 2. Shear stress-strain curves for the systems reinforced with (a) shorter and (b) longer diblock rings (solid lines) and diblock linear chains (dashed lines). In each panel, the curves for the immiscible interface and the bulk are added for comparisons. The diblock copolymers across the interfaces (dashed black lines) at $\gamma = 0$ are visualized. One diblock ring and a pair of neighboring diblock linear chains are visualized in each panel.

immiscible interface, indicating the lack of interfacial entanglements. By contrast, $\rho_{\rm K}$ is uniform across the well-entangled bulk sample.

The shear stress-strain curves for all systems reinforced with diblock copolymers are shown in Figure 2. The initial elastic response and yielding of all these systems agree with those for the immiscible interface and the bulk. The hardening modulus for the postyield regime, as reflected in the slope of the stressstrain curve at large γ , is lower for shorter diblock copolymers (Figure 2a), while elevated and closer to the bulk value for longer diblock copolymers (Figure 2b). For both diblock rings and diblock linear chains, σ_p and γ_p increase with increasing M_{db} , indicating that the adhesion is enhanced as the concentration of diblock copolymers increases. Another major trend is that the system reinforced with diblock rings have larger σ_p and γ_p than the corresponding system reinforced with diblock linear chains at the same coverage. This trend indicates the adhesion is enhanced when ring topology replaces the linear topology of the diblock copolymers. The strongest adhesion is observed for R200-240, with σ_p and γ_p reaching 0.92 and 0.96 of their respective bulk values.

The greater effectiveness of diblock rings than diblock linear chains in strengthening the immisible interface arises from the threading of diblock rings by linear chains from opposite sides. The threading events are identified by calculating the Gauss Linking Number (GLN). Consider two curves l_1 and l_2 with parametrizations $\gamma_1(t)$ and $\gamma_2(s)$, where $0 \le t \le 1$ and $0 \le s \le 1$. The GLN is defined as a double integral

$$L(l_1, l_2) = \frac{1}{4\pi} \int_0^1 \int_0^1 [(\dot{\gamma}_1(t), \dot{\gamma}_2(s), \gamma_1(t) - \gamma_2(s)) / ||\gamma_1(t) - \gamma_2(s)||^3] dt ds$$
(1)

where $(\dot{\gamma}_1(t),\dot{\gamma}_2(s),\gamma_1(t)-\gamma_2(s))$ is the scalar triple product. For two closed loops, the GLN is an integer representing the number of times that one curve winds around the other and may be positive or negative depending on the orientation of the two curves. The GLN becomes a noninteger number if at least one curve is open. The calculations of the GLN were done using a modified version of the TEPPP (Topological Entanglement in Polymers, Proteins and Periodic Structures) software that can work for mixtures of ring and linear polymers.

For a pair of polymers consisting of a diblock ring and a linear chain, the criterion for the ring to be threaded by the linear chain is that the absolute value of the GLN is greater than 0.5. As shown by a recent study, ¹⁵ GLN with absolute value of 0.5 corresponds to a linear chain which is just beginning to penetrate a ring polymer. Moreover, the

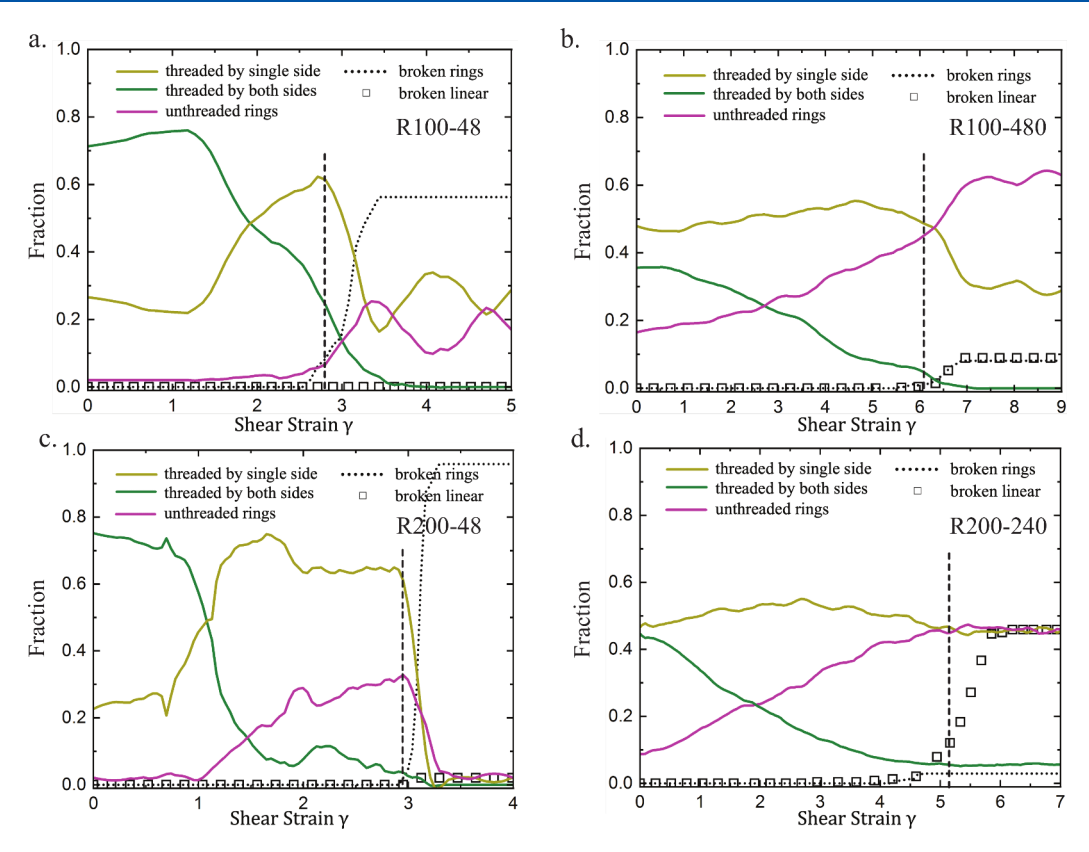


Figure 3. Evolution of the fractions of diblock rings in different categories with increasing γ for (a) R100-48, (b) R100-480, (c) R200-48, and (d) R200-240. The open symbols indicate the fraction of broken linear homopolymers as a function of γ . The dashed vertical line indicates γ_p in each panel. Each original data point has been replaced with the average of neighboring data points within the span of $\Delta \gamma = 1$ (a–c) and 2 (d).

distribution of absolute GLN values has a local minimum near 0.5. Perturbing the threashold value around 0.5 does not significantly affect the topological analysis. Using this GLNbased criterion, the diblock rings in each system are classified into 3 categories: threaded by linear chains from both sides (double-threaded), threaded by linear chains from only one side (single-threaded), and not threaded at all (unthreaded). Under shear deformation, a diblock ring may be broken due to bond breaking, resulting in another category, broken diblock rings. The fractions of diblock rings in different categories evolve with increasing shear strain, as shown in Figure 3 for each system. For R100-48 at $\gamma = 0$, the fractions of double-threaded, single-threaded, and unthreaded rings are 0.73, 0.25, and 0.02, respectively. Upon shearing, the fractions vary slowly until $\gamma \approx$ 1.5. Further shearing leads to a reduction in the fraction of double-threaded rings and an increase in the fraction of singlethreaded rings, indicating the dethreading of diblock rings. Around the failure strain γ_p , the fraction of double-threaded rings continues to decrease. Meanwhile, the fraction of singlethreaded rings sharply decreases, whereas the fractions of unthreaded rings and broken rings rise.²⁹ The final fractions of double-threaded, single-threaded, unthreaded, and broken rings are 0, 0.15, 0.29, and 0.56. The evolutions of selected diblock rings in R100-48 with increasing γ are visualized in Figures S2a,b. Apart from the diblock rings, none of the immiscible linear polymer chains have broken by the end of the shearing. As a result, the breaking of diblock rings threaded by linear chains from both sides of the interface is the dominant failure mechanism for R100-48.

The higher coverage of the interface by diblock rings in R100-480 compared to that in R100-48 alters the fractions of

rings in different topology categories at $\gamma = 0$. As shown in Figure 3b, the fractions of double-threaded, single-threaded, and unthreaded rings for R100-480 are 0.35, 0.48, and 0.17, respectively. Both the fractions of unthreaded and singlethreaded rings increase compared to R100-48 because the diblock rings compete for the nearby linear chains to form ring-linear threading. The contrast between the monomer density profiles at low (Figure S1b) and high (Figure S1c) coverages show the exclusion of linear homopolymer chains from the interface with increasing coverage of diblock rings. At high coverage, the concentration of linear chains surrounding the diblock rings is insufficient to ensure all rings are threaded. From the initial state, the fractions of the three types of rings remain almost unchanged until $\gamma \approx 1$. With increasing γ , the fraction of double-threaded rings decreases, while the fraction of single-threaded rings slightly increases and the fraction of unthreaded rings increases more rapidly. As shear strain exceeds γ_p , the fraction of double-threaded rings drops to 0, the fraction of single-threaded rings sharply drops to 0.28, whereas the fraction of unthreaded rings rises to 0.63 together with a fraction of 0.09 broken rings. By $\gamma = 9$, the fraction of broken homopolymer chains is 0.09. The fraction of broken bonds out of all bonds in the homopolymers is $f_{\text{broken}} = 7.64 \times 10^{-5}$, which is well below 2.73×10^{-4} for the bulk failure (Figure 1a). In short, the unthreading of diblock rings by linear chains becomes the dominant failure mechanism for R100-480.

At the lower coverage of diblock rings with $M_{db}=48$, as the diblock ring length increases from $N_{db}=100$ to $N_{db}=200$, the fractions of rings in the three topology categories remain almost unchanged at $\gamma=0$, as seen by comparing Figure 3a and c. Upon shearing, the dominant failure mechanism is still the

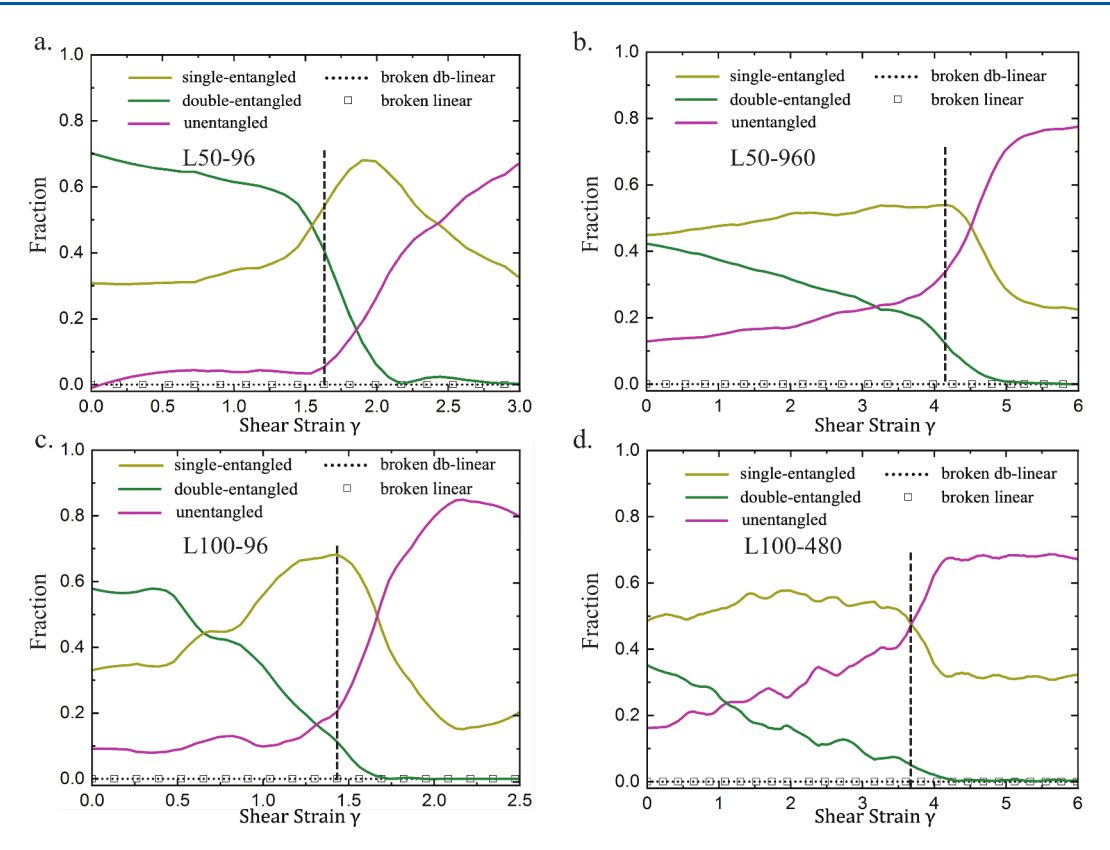


Figure 4. Evolution of the fractions of diblock linear chains in different categories with increasing γ for (a) L50-96, (b) L50-960, (c) L100-96, and (d) L100-480. The open symbols indicate the fraction of broken linear homopolymers as a function of γ . The dashed vertical line in each pane indicates γ_p . Each original data point has been replaced with the average of neighboring data points within the span of $\Delta \gamma = 1$.

breaking of diblock rings, and γ_p is almost the same for the two values of N_R . However, the fraction of broken rings at the end of the shearing increases from 0.56 for $N_{db}=100$ to 0.96 for $N_{db}=200$. This increase agrees with the higher hardening modulus and thus higher σ_p as N_R doubles.

For longer diblock rings with $N_{db} = 200$, as the number of rings increases from $M_{db} = 48$ to $M_{db} = 240$, the fractions of unthreaded and single-threaded rings at $\gamma = 0$ increase, as shown by Figures 3c and 3d. This change induced by the increase in the coverage of rings is similar to that from R100-48 to R100-480. It results from the fact that on average fewer linear chains are available to thread a ring, as linear chains are excluded from the interface with increasing coverage of diblock rings (see the monomer density profiles in Figures S1d,e). At the end of shearing R200-240, the fraction of single-threaded and unthreaded rings are 0.53 and 0.4, while the fraction of broken rings is only 0.03. Figure S2c-e illustrate the dethreading of selected diblock rings in R200-240. By the end of the shearing, the fraction of broken homopolymer chains is 0.46. The fraction of broken bonds in the homopolymers is $f_{\text{broken}} = 1.49 \times 10^{-4}$, which is on the same order of 2.73×10^{-4} for the bulk failure. These results show that the diblock rings in R200-240 have effectively stitched the immiscible chains for enhanced adhesion.

Diblock linear chains are less effective in reinforcing the immiscible polymer interface, because the entanglements between the blocks and the two sides of the interface are more easily released upon shearing. The entanglements between a diblock linear chain and the surrounding homopolymer chains are characterized based on the GLN calculation. A diblock linear chain is considered to be

entangled with a homopolymer chain if the GLN between the two chains has an absolute value greater than 0.5. The GLN with absolute value of 0.5 corresponds to two linear chains beginning to impinge on each other. Similar to the topological analysis of diblock rings, diblock linear chains at γ = 0 are grouped into 3 categories: double-entangled, singleentangled, and unentangled, which correspond to entanglements with both sides, only one side, and no side at all, respectively. Figure 4 shows the fractions of diblock linear chains in different categories vary with N_{db} and M_{db} , similar to the variations of diblock rings in different topological categories (Figure 3). In all cases, the fraction of double-entangled linear chains decreases, while the fractions of single-entangled and unentangled linear chains increase with increasing shear strain. As γ increases above γ_{ν} , no diblock linear chains are doubleentangled. Most diblock linear chains are unentangled, with the rest only single-entangled. Meanwhile, no bonds are broken by the end of the shearing for L50-96, L50-960, and L100-96, and only a small fraction of bonds in homopolymer chains are broken ($f_{\text{broken}} = 9.05 \times 10^{-6}$) for L100-480. As a result, the failure mechanism of the systems reinforced with diblock linear chains is the disentanglement of diblock linear chains from the two immiscible polymers.

The simulation data for the diblock ring systems suggest two necessary conditions for the recovery of the bulk mechanics at the interface. The first condition is that the diblock rings should be sufficiently long to recover the bulk strain-hardening behavior. The strain hardening modulus, as reflected in the slope of the postyield shear stress-strain curve (Figure 2), is lower for R100 while close to the bulk value for R200. With a reduced strain hardening modulus, the bulk shear stress cannot

be recovered at any large shear strain. This condition is ultimately rooted in the molecular weight dependence of the strain-hardening behavior of glassy polymers. The second condition is that the diblock rings should be above the overlap condition, i.e., $\Omega > 1$. This condition is implied by the comparison of diblock rings at two coverages with different values of Ω in Figure 2. As listed in Table S1, $\Omega = 0.2$, 1.3, 0.4, and 1.6 for R100-48, R100-480, R200-48, and R200-240, respectively. The diblock rings at high coverage with $\Omega > 1$ ensure no interfacial region exists where stress cannot be transferred from one side to the other, bringing the interfacial mechanics closer to the bulk mechanics. To quantitatively determine and understand the sufficient conditions for the recovery of bulk mechanics with diblock ring adhesives, one would need more extensive simulations and theoretical analysis.

In summary, the molecular simulations and topological analysis have demonstrated ring-linear threading between diblock ring polymers and surrounding linear chains as a new microscopic mechanism for reinforcing immiscible polymer interfaces. The two extra bonds in a diblock ring compared to a pair of diblock linear chains effectively alters the failure mechanism and increases both σ_p and γ_p . Diblock linear chains at an immiscible polymer interface may be disentangled from both sides upon deformation, while diblock rings are threaded by linear chains from both sides, creating a microscopic version of Velcro tapes. The resulting systems fail predominantly by the breaking of diblock rings at low coverage, whereas by the breaking of homopolymer chains at high coverage, as in the bulk. It is anticipated that experimentalists may be motivated to combine topological chemistry tools^{30–32} and mechanical engineering techniques³³ to create the systems simulated here and verify diblock rings as effective topological adhesives. Future work may also explore the transformative capability of diblock rings in reinforcing immiscible polymer interfaces of block copolymer-homopolymer blends in various equilibrium phases. 34,35

ASSOCIATED CONTENT

Supporting Information

The Supporting Information is available free of charge at https://pubs.acs.org/doi/10.1021/acsmacrolett.4c00446.

Density profiles of monomers, visualizations of failure mechanisms, and the table listing the radius of gyration components $R_{g,x}$, $R_{g,y}$, and $R_{g,z}$, the average spacing d between diblock copolymers, and the overlap parameter $\Omega = \pi R_{g,x} R_{g,y} / d^2$ (PDF)

AUTHOR INFORMATION

Corresponding Author

Ting Ge — Department of Chemistry and Biochemistry, University of South Carolina, Columbia, South Carolina 29208, United States; orcid.org/0000-0003-2456-732X; Email: tingg@mailbox.sc.edu

Authors

Andrew Wijesekera – Department of Chemistry and Biochemistry, University of South Carolina, Columbia, South Carolina 29208, United States; orcid.org/0009-0006-1591-9046

- Daniel L. Vigil Sandia National Laboratories, Albuquerque, New Mexico 87185, United States; orcid.org/0000-0001-9860-0888
- Gary S. Grest Sandia National Laboratories, Albuquerque, New Mexico 87185, United States; orcid.org/0000-0002-5260-9788
- Siteng Zhang Department of Chemistry and Biochemistry, University of South Carolina, Columbia, South Carolina 29208, United States

Complete contact information is available at: https://pubs.acs.org/10.1021/acsmacrolett.4c00446

Notes

The authors declare no competing financial interest.

ACKNOWLEDGMENTS

We thank T. C. O'Connor for helpful discussions. T.G. acknowledges start-up funds from the University of South Carolina and the National Science Foundation CAREER award DMR-2236693. Computational resources were provided by University of South Carolina flagship computing cluster Hyperion. This work was performed, in part, at the Center for Integrated Nanotechnologies, an Office of Science User Facility operated for the U.S. Department of Energy (DOE) Office of Science. Sandia National Laboratories is a multimission laboratory managed and operated by National Technology and Engineering Solutions of Sandia, LLC, a wholly owned subsidiary of Honeywell International, Inc., for the U.S. DOE's National Nuclear Security Administration under Contract No. DE-NA-0003525. The views expressed in the paper do not necessarily represent the views of the U.S. DOE or the U.S. Government.

REFERENCES

- (1) Helfand, E.; Tagami, Y. Theory of the Interface between Immiscible Polymers II. J. Chem. Phys. 1972, 56, 3592.
- (2) Wool, R. P. Polymer Interfaces: Structure and Strength; Hanser: Munich, 1995.
- (3) Jones, R. A. L.; Richards, R. W. Polymers at Surfaces and Interfaces; Cambridge University Press: New York, 1999.
- (4) Raos, G.; Zappone, B. Polymer Adhesion: Seeking New Solutions for an Old Problem. *Macromolecules* **2021**, *54*, 10617.
- (5) Creton, C.; Kramer, E. J.; Hui, C.-Y.; Brown, H. R. Failure Mechanisms of Polymer Interfaces Reinforced with Block Copolymers. *Macromolecules* **1992**, *25*, 3075–3088.
- (6) Dai, C.-A.; Jandt, K. D.; Iyengar, D. R.; Slack, N. L.; Dai, K. H.; Davidson, W. B.; Kramer, E. J.; Hui, C.-Y. Strengthening Polymer Interfaces with Triblock Copolymers. *Macromolecules* **1997**, *30*, 549–560
- (7) Zhang, J.; Cole, P. J.; Nagpal, U.; Macosko, C. W.; Lodge, T. P. Direct correlation between adhesion promotion and coupling reaction at immiscible polymer-polymer interfaces. *J. Adhes.* **2006**, *82*, 887–902.
- (8) Eagan, J. M.; Xu, J.; Di Girolamo, R.; Thurber, C. M.; Macosko, C. W.; La Pointe, A. M.; Bates, F. S.; Coates, G. W. Combining polyethylene and polypropylene: Enhanced performance with PE/iPP multiblock polymers. *Science* **2017**, 355, 814–816.
- (9) Ivancic, R. J. S.; Audus, D. J. Predicting compatibilized polymer blend toughness. *Science Advances* **2024**, *10*, No. eadk6165.
- (10) Collanton, R. P.; Dorfman, K. D. Deformation and failure of glassy polymer-polymer interfaces compatibilized by linear multiblock copolymers. *Physical Review Materials* **2024**, *8*, 075604.
- (11) Edgecombe, B. D.; Stein, J. A.; Frechet, J. M. J.; Xu, Z.; Kramer, E. J. The Role of Polymer Architecture in Strengthening Polymer-Polymer Interfaces: A Comparison of Graft, Block, and Random

- Copolymers Containing Hydrogen-Bonding Moieties. *Macromolecules* **1998**, *31*, 1292–1304.
- (12) Chen, Z.; Steinmetz, C.; Hu, M.; Coughlin, E. B.; Wang, H.; Heller, W. T.; Bras, W.; Russell, T. P. Star Block Copolymers at Homopolymer Interfaces: Conformation and Compatibilization. *Macromolecules* **2023**, *56*, 8308–8322.
- (13) Parisi, D.; Ahn, J.; Chang, T.; Vlassopoulos, D.; Rubinstein, M. Stress Relaxation in Symmetric Ring-Linear Polymer Blends at Low Ring Fractions. *Macromolecules* **2020**, *53*, 1685–1693.
- (14) O'Connor, T. C.; Ge, T.; Grest, G. S. Composite entanglement topology and extensional rheology of symmetric ring-linear polymer blends. *J. Rheol.* **2022**, *66*, 49–65.
- (15) Vigil, D. L.; Ge, T.; Rubinstein, M.; O'Connor, T. C.; Grest, G. S. Measuring topological constraint relaxation in ring-linear polymer blends. *Phys. Rev. Lett.* **2024**, *133*, 118101.
- (16) Pyromali, C.; Patelis, N.; Cutrano, M.; Gosika, M.; Glynos, E.; Moreno, A. J.; Sakellariou, G.; Smrek, J.; Vlassopoulos, D. Nonmonotonic Composition Dependence of Viscosity upon Adding Single-Chain Nanoparticles to Entangled Polymers. *Macromolecules* **2024**, *57*, 4826–4832.
- (17) Kremer, K.; Grest, G. S. Dynamics of entangled linear polymer melts: A molecular-dynamics simulation. *J. Chem. Phys.* **1990**, 92, 5057–5086.
- (18) Grest, G. S. Communication: Polymer entanglement dynamics: Role of attractive interactions. *J. Chem. Phys.* **2016**, *145*, 141101.
- (19) Ge, T.; Robbins, M. O.; Perahia, D.; Grest, G. S. Healing of Polymer Interfaces: Interfacial Dynamics, Entanglements, and Strength. *Phys. Rev. E* **2014**, *90*, 012602.
- (20) Sides, S. W.; Grest, G. S.; Stevens, M. J.; Plimpton, S. J. Effect of End-Tethered Polymers on Surface Adhesion of Glassy Polymers. *J. Polym. Sci., Part B: Polym. Phys.* **2004**, 42, 199–208.
- (21) Thompson, A. P.; Aktulga, H. M.; Berger, R.; Bolintineanu, D. S.; Brown, W. M.; Crozier, P. S.; in 't Veld, P. J.; Kohlmeyer, A.; Moore, S. G.; Nguyen, T. D.; Shan, R.; Stevens, M. J.; Tranchida, J.; Trott, C.; Plimpton, S. J. LAMMPS-a flexible simulation tool for particle-based materials modeling at the atomic, meso, and continuum scales. *Comput. Phys. Commun.* **2022**, 271, 108171.
- (22) Wijesekera, A.; Vigil, D. L.; Ge, T. Molecular Simulations Revealing Effects of Non-concatenated Ring Topology on Phase Behavior of Symmetric Diblock Copolymers. *Macromolecules* **2024**, *57*, 5092–5104.
- (23) Ge, T.; Pierce, F.; Perahia, D.; Grest, G. S.; Robbins, M. O. Molecular dynamics simulations of polymer welding: Strength from interfacial entanglements. *Phys. Rev. Lett.* **2013**, *110*, 098301.
- (24) Wang, J.; Ge, T. Crazing reveals an entanglement network in glassy ring polymers. *Macromolecules* **2021**, *54*, 7500–7511.
- (25) Wang, J.; O'Connor, T. C.; Grest, G. S.; Ge, T. Super-stretchable Elastomer from Cross-linked Ring Polymers. *Phys. Rev. Lett.* **2022**, *128*, 237801.
- (26) Ge, T.; Grest, G. S.; Robbins, M. O. Structure and Strength at Immiscible Polymer Interfaces. ACS Macro Lett. 2013, 2, 882–886.
- (27) Kröger, M.; Dietz, J. D.; Hoy, R. S.; Luap, C. The Z1+ package: Shortest multiple disconnected path for the analysis of entanglements in macromolecular systems. *Comput. Phys. Commun.* **2023**, 283, 108567.
- (28) Herschberg, T.; Pifer, K.; Panagiotou, E. A computational package for measuring Topological Entanglement in Polymers, Proteins and Periodic systems (TEPPP). *Comput. Phys. Commun.* **2023**, 286, 108639.
- (29) For $\gamma > 3.5$, the nonmonotonic variation of the fraction of the rings threaded by a single side is related to the sliding process at the fractured interface. Polymers at the fractured interface are aligned with the shearing direction. A small displacement normal to the shearing direction may result in the disappearance or reemergence of a threading event defined based on the sharp threshold that the absolute value of GLN = 0.5.
- (30) Lin, Y.; Zhang, Y.; Wang, Z.; Craig, S. L. Dynamic Memory Effects in the Mechanochemistry of Cyclic Polymers. *J. Am. Chem. Soc.* **2019**, *141*, 10943–10947.

- (31) Haque, F. M.; Grayson, S. M. The synthesis, properties and potential applications of cyclic The synthesis, properties and potential applications of cyclic polymers. *Nat. Chem.* **2020**, *12*, 433–444.
- (32) Romio, M.; Trachsel, L.; Morgese, G.; Ramakrishna, S. N.; Spencer, N. D.; Benetti, E. M. Topological Polymer Chemistry Enters Materials Science: Expanding the Applicability of Cyclic Polymers. *ACS Macro Lett.* **2020**, *9*, 1024–1033.
- (33) Steck, J.; Yang, J.; Suo, Z. Covalent Topological Adhesion. ACS Macro Lett. 2019, 8, 754–758.
- (34) Vorselaars, B.; Spencer, R. K. W.; Matsen, M. W. Instability of the Microemulsion Channel in Block Copolymer Homopolymer Blends. *Phys. Rev. Lett.* **2020**, *125*, 117801.
- (35) Spencer, R. K. W.; Matsen, M. W. Coexistence of Polymeric Microemulsion with Homopolymer-Rich Phases. *Macromolecules* **2021**, *54*, 1329–1337.